

Distributions of the largest fragment size in multifragmentation: Traces of a phase transition

J. Brzychczyk,* T. Pietrzak, and A. Wieloch

M. Smoluchowski Institute of Physics, Jagiellonian University, Pl-30-348 Kraków, Poland

W. Trautmann

GSI Helmholtzzentrum für Schwerionenforschung GmbH, D-64291 Darmstadt, Germany

(Dated: June 30, 2021)

Abstract

Distributions of the largest fragment charge are studied using the ALADIN data on fragmentation of ^{197}Au projectiles at relativistic energies. The statistical measures skewness and kurtosis of higher-order fluctuations provide a robust indication of the transition point, linked to a phase transition in the thermodynamic limit. Extensive comparisons with predictions of a bond percolation model corroborate the high accuracy of this model in reproducing the distributions as well as the whole fragmentation pattern as represented by the measured charge correlations. In analogy to percolation, the pseudocritical and critical points are identified in the fragmentation data. Questions concerning the distinction between different models and between first- and second-order phase transitions are discussed.

PACS numbers: 25.70.Pq, 24.60.Ky, 05.70.Fh, 05.70.Jk, 64.60.Ak

* janusz.brzychczyk@uj.edu.pl

I. INTRODUCTION

In nuclear multifragmentation studies, the mass of the largest fragment and its distribution have received special attention. The largest fragment is often identified with the liquid phase in a mixed-phase configuration and thus assumed to play the role of the order parameter in a liquid-gas phase-transition scenario. Its distributions are expected to provide valuable insight into the phase behavior of the investigated systems [1–10]. A transition from a “liquid” to a “gaseous” state is associated with a rapid decrease of the largest fragment size. It may correspond to the order-parameter discontinuity in the case of a first-order phase transition or to the power-law disappearance near a second-order transition point (a critical point). Besides the characteristic evolution of its mean-value, event-to-event fluctuations reflected in the probability distribution of the largest fragment size are of considerable interest. Experimental examinations have focused on the appearance of particularly large fluctuations [6, 9, 11–15], on bimodal characteristics representative of a two-phase coexistence [6, 8, 10, 16–18], on so-called Δ -scaling features [1, 5, 6, 8], and on the connection with dynamical observables as, e.g., radial flow [19].

Although the presence of a phase transition is often deduced, its kind is usually not unambiguously identified. In small systems the asymptotic behavior is strongly modified by finite size and surface effects, so that the distinction between first- and second-order phase transitions becomes very difficult. Simulations with lattice gas models have shown that critical-like features are observed in finite systems not only along the Kertész line [20, 21] but also inside the liquid-gas coexistence region, i.e. the first order phase transition can mimic critical behavior [3, 7, 22–24]. Moreover, the control parameter, the temperature or energy content in a thermodynamical phase transition, cannot be precisely measured and must be substituted by a another measurable quantity. Sorting events according to a substitute control parameter will additionally blur the observed signals.

The present work is motivated by percolation studies suggesting new signatures of a critical behavior associated with the distribution properties of the largest fragment size or mass [25]. They are exhibited by the cumulant ratios up to fourth order, i.e. the normalized variance, skewness and kurtosis. Specific features of these dimensionless cumulants characterizing the distribution provide a robust indication of the pseudocritical point in finite systems and permit estimates of the location of the critical point in the continuous

limit. Fluctuation observables up to fourth order have also been proposed for probing the QCD chiral transition and for searching for the QCD critical point with experimental data at much higher energies [26, 27]. They are presently widely used to characterize the hot medium generated in ultra-relativistic heavy-ion collisions [28, 29]. The rich phenomenology of fluctuation observables near a critical point has recently been explored in a description of the liquid-gas phase transition of nuclear matter with a model based on the Van-der-Waals equation [30].

These new signatures are applicable to very small systems and can be tested with various measurable sorting variables. Therefore, they are well suited for an application to nuclear multifragmentation. Within this context, properties of the largest fragment size in multifragmentation are investigated using the results of the ALADIN Collaboration [31]. In addition, comparisons between predictions of a bond percolation model and the experimental data are not restricted to the largest fragment characteristics [32]. The whole fragmentation pattern is verified in detail to obtain a quantitative reference, permitting comparisons with other models representing alternative multifragmentation scenarios.

A brief recall of the main cumulant features near the percolation transition is given in the next section. To obtain some information on the question of their uniqueness or universality, percolation results are compared with predictions of a thermodynamic model known to contain a first-order phase transition [16, 33, 34].

II. DISTRIBUTION OF THE LARGEST FRAGMENT SIZE

Percolation calculations presented in [25] and in this work are performed with a three-dimensional bond percolation model on simple cubic lattices [35, 36]. Events are generated using a Monte Carlo procedure. The sites are arranged on the lattice in the most compact configuration, the bonds are created randomly with probability p . Clusters are recognized with the Hoshen-Kopelman algorithm [37]. Free boundary conditions are applied to account for the presence of surface in real systems.

Given a control parameter value p and the total number of sites A_0 (the system size), the probability distribution $P(A_{max})$ of the largest cluster size A_{max} is determined from a large sample of events. The statistical measures as the mean, variance, skewness and kurtosis contain the most significant information about the distribution. Of particular interest are

the following dimensionless cumulant ratios

$$\begin{aligned}
K_2 &\equiv \mu_2 / \langle A_{max} \rangle^2 = \kappa_2 / \kappa_1^2 \\
K_3 &\equiv \mu_3 / \mu_2^{3/2} = \kappa_3 / \kappa_2^{3/2} \\
K_4 &\equiv \mu_4 / \mu_2^2 - 3 = \kappa_4 / \kappa_2^2,
\end{aligned} \tag{1}$$

where $\langle A_{max} \rangle$ denotes the mean value, $\mu_i = \langle (A_{max} - \langle A_{max} \rangle)^i \rangle$ is the i th central moment, and κ_i is the i th cumulant of $P(A_{max})$. K_2 is the variance normalized to the squared mean, K_3 is the skewness which indicates the distribution asymmetry, and K_4 is the kurtosis excess measuring the degree of peakedness. The cumulants are simple functions of the central moments with $\kappa_1 = \langle A_{max} \rangle$, $\kappa_2 = \mu_2$, $\kappa_3 = \mu_3$, and $\kappa_4 = \mu_4 - 3\mu_2^2$. In the transition region, these quantities obey with good accuracy finite-size scaling relations even for very small systems with open boundaries [25]. This permits the identification of universal (independent of the system size) features of K_i at the transition point or region.

This form of universality can be illustrated with the help of Fig. 1(a). The cumulant ratios K_i are plotted as a function of the bond breaking probability $p_b \equiv 1 - p$ for three different system sizes. Increasing p_b corresponds to increasing the temperature in a physical application that contains temperature as a control parameter, as it is the case here for nuclear multifragmentation. The location of the critical point in the continuous limit $p_c \simeq 0.751$ is marked by the vertical long line. According to finite-size scaling, the values of the cumulants K_i at p_c are expected to be independent of the system size. This is quite precisely observed in Fig. 1(a) as the crossing of the curves. A prominent feature of K_2 is its maximum located very close to p_c . Maxima of other quantities used as criticality signals show much larger deviations from p_c (e.g., the maximum variance of the fragment mass distribution, see examples given in Ref. [25]). The transition point in finite systems can be associated with the broadest and most symmetric $P(A_{max})$ distribution observed near the pseudocritical point defined by the maximum of the mean cluster size being the analog of the susceptibility [25]. This transitional distribution is indicated by $K_3 = 0$ and the minimum value of K_4 of about -1 . Figure 2(a) shows examples of such distributions. The distance of the pseudocritical point from p_c increases with decreasing system size according to finite-size scaling (Fig. 1(a)).

The cumulant features characterizing the critical and pseudocritical points are approximately preserved for the corresponding points when events are sorted by measurable variables correlated with the control parameter, such as the total multiplicity or the total mass

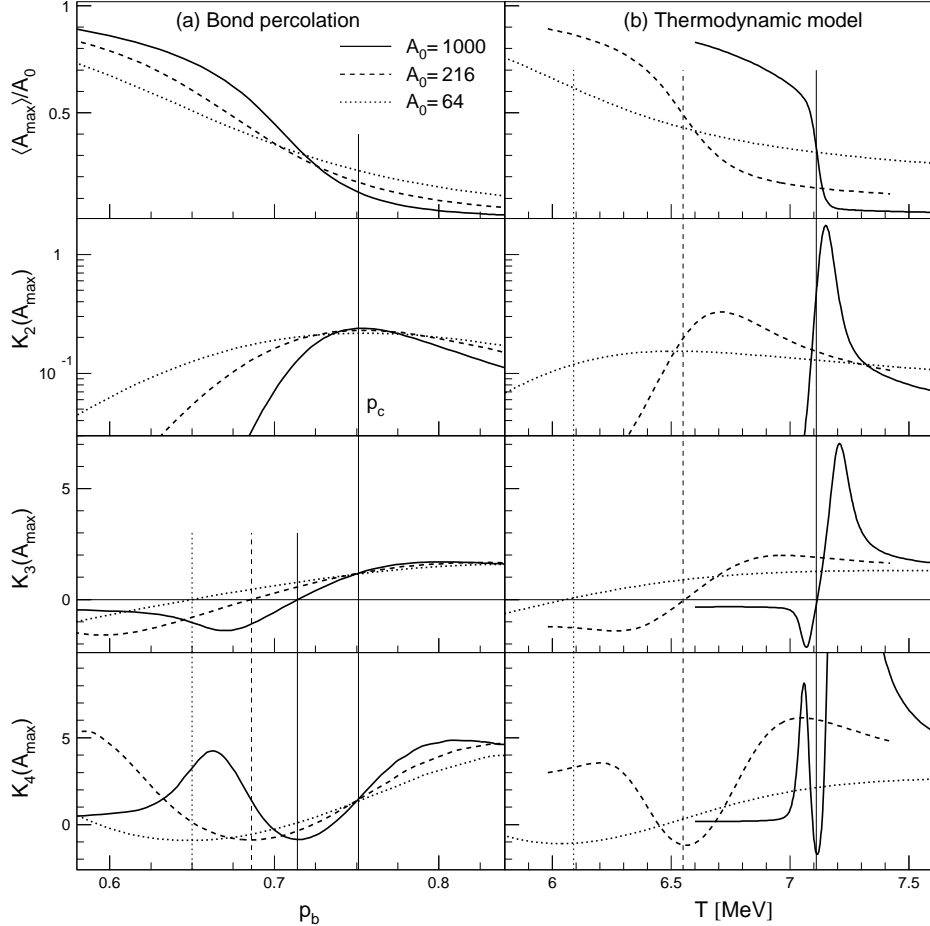


FIG. 1. The cumulants of Eqs. (1) for three different system sizes. (a) Percolation results plotted as a function of the bond breaking probability. The long vertical line indicates the critical point p_c in the continuous limit. The short lines indicate the transition (pseudocritical) points for the finite systems. (b) Results of the thermodynamic model as a function of the temperature. The vertical lines mark the transition temperatures corresponding to the maximum specific heats of the three systems. For $A_0 = 1000$, the kurtosis excess K_4 reaches a maximum value 78 at $T \simeq 7.2$ MeV (bottom right panel).

of complex fragments. Near-critical events are indicated by the maximum of K_2 while events associated with the pseudocritical point are characterized by $K_3 = 0$ and the minimum value of K_4 of about -1 .

It is instructive to compare the percolation results with predictions of the thermodynamic model [33] which is a simplified version of the statistical multifragmentation model (SMM, Ref. [38]). The calculations have been performed for the canonical ensemble of noninteracting

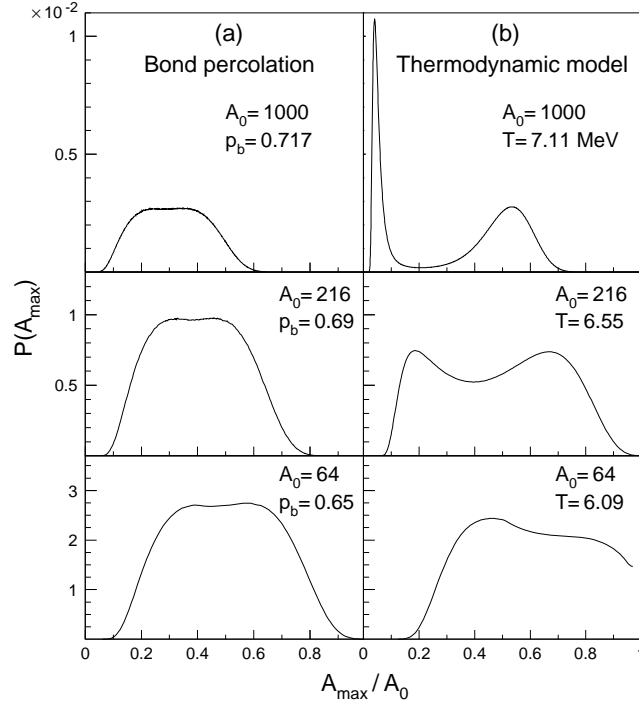


FIG. 2. Probability distributions of the largest fragment size at the transition points.

one-component fragments. The model permits computing the partition function, and thus to obtain the thermodynamic properties of the system. The presence of a first-order phase transition is well established [33, 34, 39]. The results for a freeze-out density of one third of the normal nuclear density are presented in Fig. 1(b). The transition temperatures for systems with 64, 216, and 1000 nucleons, derived from the locations of the specific heat maximum, are 6.09, 6.55, and 7.11 MeV, respectively. These values are marked by the vertical lines. In the thermodynamic limit, the maximum location is expected at $T \simeq 8$ MeV as calculated within the grand canonical approach and shown in Fig. 4 of Ref. [39]. In this model, the critical temperature is assumed to be $T_c = 18$ MeV.

As can be seen in the top diagram of Fig. 1(b), $\langle A_{\max} \rangle$ shows the fastest decrease at the transition point. A step discontinuity develops with increasing system size [33]. Similarly to the case of percolation, the transition point is precisely indicated by $K_3 = 0$ and the minimum of K_4 . Here, K_4 reaches somewhat lower values, suggesting a bimodal structure of the probability distribution as expected for a first-order phase transition in the canonical ensemble. Figure 2(b) shows that, for a system as large as $A_0 = 1000$, a distinct bimodality is observed. The two-peak structure gradually vanishes as the system size decreases.

The above examples illustrate that the transition point in small systems, associated with a phase transition in the thermodynamic limit, is well indicated by $K_3 = 0$ together with a minimum of K_4 for both, i.e. first- and second-order, types of transition. The comparisons suggest that some evidence for the transition order can be obtained from the evolution of $P(A_{max})$ with the system size. In particular, in the vicinity of the transition point the cumulants exhibit maxima whose amplitudes increase with the system size in the case of the thermodynamic model. This is in contrast to percolation where the amplitudes are bounded according to the second-order finite-size scaling.

III. EXPERIMENTAL DATA

The present work examines the ALADIN data on fragmentation of projectile spectators in $^{197}\text{Au} + \text{Cu}$, In , Au peripheral collisions at the incident energies of $600A$ MeV (Cu , In , Au targets), $800A$ MeV (Au), and $1000A$ MeV (Cu , Au). Details of the experiment and general characteristics of the data have been presented in Ref. [31]. Fragments with the atomic numbers $Z \geq 2$ were detected with high efficiencies, close to 100% at the bombarding energy of 1000 MeV/nucleon, and fully Z -identified. For the present work, the event-sorted data files were used that formed the basis of the results reported in the experimental paper [31]. The magnitude of potential effects caused by the minute but finite acceptance losses on higher-order correlations were investigated and results will be shown below.

It is a prominent feature of the data that the fragment multiplicities and correlations are independent of the projectile energy and the target nucleus when plotted as a function of Z_{bound} . This universality has been interpreted as indicating a high degree of equilibration attained prior to or during the fragmentation stage [31]. The quantity Z_{bound} is defined as the sum of the atomic numbers Z of all fragments with $Z \geq 2$. It serves as a sorting variable, correlated with the size of the projectile spectator and inversely correlated with the excitation energy per nucleon [40].

The correlation between the largest fragment charge, Z_{max} , and Z_{bound} is illustrated in Fig. 3. All the studied data sets are included. At low excitation energies, corresponding to largest Z_{bound} values, evaporation processes are dominant (events with one large fragment). There is also a small fraction of fission events with Z_{max} around 40. At excitation energies approaching and exceeding the nuclear binding energy ($Z_{\text{bound}} < 40$), the systems are dis-

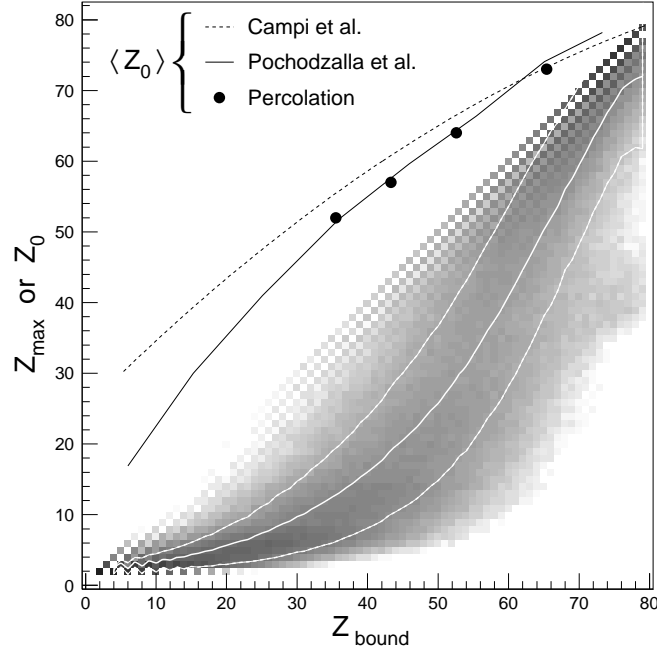


FIG. 3. Distribution of Z_{\max} vs Z_{bound} for the ALADIN data (with shadings in a logarithmic scale). The solid white line shows the mean values of Z_{\max} , the broken lines indicate the rms dispersions. The full and dashed black lines represent two estimates of the mean system size Z_0 obtained from the experimental data with different methods [41, 42] while the filled circles give the result obtained with percolation (see text).

assembled into many small fragments. The transition between the two extreme regimes is characterized by a rapidly decreasing Z_{\max} associated with an increasing number of fragments.

Experimental information on the size of the fragmenting system (spectator remnant) is important for testing theoretical predictions. An estimation of the mean system mass $\langle A_0 \rangle$ as a function of Z_{bound} in several Z_{\max} windows was made for the 600A MeV $^{197}\text{Au} + \text{Cu}$ reaction [41]. Assuming the charge-to-mass ratio $Z_0/A_0 = 0.4$, the value of ^{197}Au projectiles, the results converted to the mean system charge $\langle Z_0 \rangle$ and averaged over Z_{\max} bins are shown in Fig. 3 by the solid line. A similar result (dashed line) was obtained by Campi *et al.* who used a sum-rule approach for extrapolating from the measured Z_{bound} to Z_0 [42].

In the present work the system sizes will be deduced from comparisons between the experimental data and the predictions of the percolation model. These results are indicated in the figure by the filled circles.

IV. PERCOLATION ANALYSIS

In the experimental data, the atomic number serves as a measure of the fragment size. The corresponding measure in the percolation analysis performed here is the number of sites contained within a cluster. In other words, the number of sites is considered as the number of proton charges. In the following, the same notation will be used for percolation quantities as for their experimental counterparts. Percolation events are generated for the bond probabilities uniformly distributed in the interval $[0, 1]$, and then sorted according to Z_{bound} .

The cumulant ratios K_i of the largest-fragment size distribution $P(Z_{\text{max}})$ are examined in Fig. 4. The percolation results are plotted in the left part as a function of Z_{bound} , normalized to the system size Z_0 , for three different system sizes that span over a range expected to be in the transition region. In this representation, the K_i distributions show a weak dependence on the system size which vanishes at the pseudocritical point located at $Z_{\text{bound}}/Z_0 \simeq 0.84$ (the squares). The results corresponding to the true critical point are located near the maximum of K_2 (cf. Fig. 1) but their positions on the Z_{bound}/Z_0 axis depend somewhat on the system size (filled circles in Fig. 4, left panel).

The experimental results are shown in the right diagrams for the $^{197}\text{Au} + ^{197}\text{Au}$ systems at 600 and 1000 MeV/nucleon and for the summed data sets (all targets and all energies). Here, the cumulant ratios K_i are plotted as a function of Z_{bound} . The system sizes are considered unknown quantities that are to be determined. The comparison of the different data sets indicates significant systematic differences only for K_2 below $Z_{\text{bound}} \simeq 50$. The statistical errors are small and comparable to the apparent scatter of the data points. They are smallest near the pseudocritical point $Z_{\text{bound}} = 54$ and there smaller than the size of the data symbols. Larger errors are expected for smaller Z_{bound} . At $Z_{\text{bound}} = 31$, e.g., the error analysis for the $^{197}\text{Au} + ^{197}\text{Au}$ system at 1000 MeV/nucleon yields 0.0091, 0.077, and 0.347 for the statistical uncertainties of K_2 , K_3 , and K_4 , respectively. For clarity, these errors are not displayed in the figure.

Overall, the percolation and experimental patterns of K_i are very similar. The specific characteristics of the percolation pseudocritical point are well observed in the data at $Z_{\text{bound}} \simeq 54$. With this correspondence, the mean system size at $Z_{\text{bound}} \simeq 54$ may be estimated as $Z_0 \simeq Z_{\text{bound}}/0.84 \simeq 64$. For the percolation “critical” point, an approximate

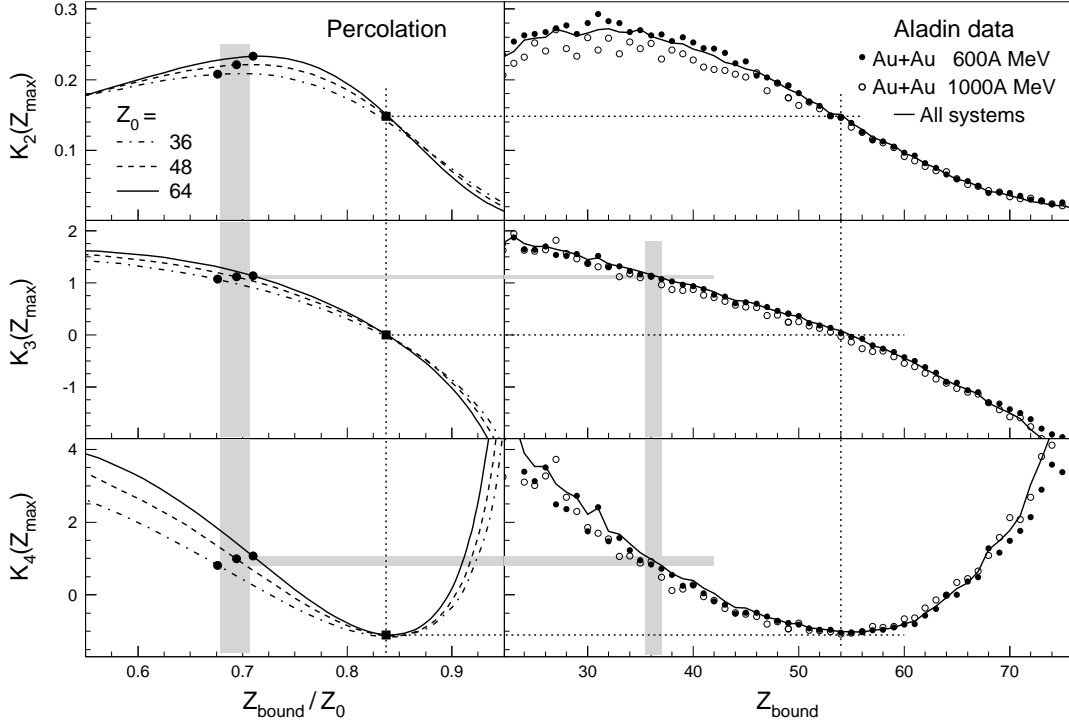


FIG. 4. The cumulants of $P(Z_{\max})$ as a function of Z_{bound} (or Z_{bound} normalized with respect to Z_0 in the case of percolation). The results of bond percolation calculations for three values of Z_0 (left panels) are shown in comparison with the experimental data for ^{197}Au fragmentation (right panels) following collisions with ^{197}Au targets at two energies (symbols) and the combined results for all systems (full lines). The meaning of the lines and of the symbols in the left panels is explained in the text. The statistical errors are of the order of the scatter of the data symbols (see text).

correspondence can be established relying on K_3 and K_4 . It indicates $Z_{\text{bound}} \simeq 36$ and a system size Z_0 around $36/0.69 \simeq 52$.

The experimental values of K_2 in the region of small Z_{bound} depend slightly on the projectile energy. It may be related to a sensitivity of K_2 to existing small changes in the reaction dynamics or perhaps simply to a residual energy dependence of the detection efficiency. At small Z_{bound} , i.e. at large excitation energies, secondary evaporation effects may also be of importance. In order to test the sensitivity of K_i to such effects a simple simulation was performed and applied to percolation events. The result is shown in Fig. 5. The largest cluster was divided into two fragments: $Z_{\text{max}} \rightarrow (Z_{\text{max}} - 1) + 1$ with probability p_1 , or $Z_{\text{max}} \rightarrow (Z_{\text{max}} - 2) + 2$ with probability p_2 . Such calculations with various assumptions on

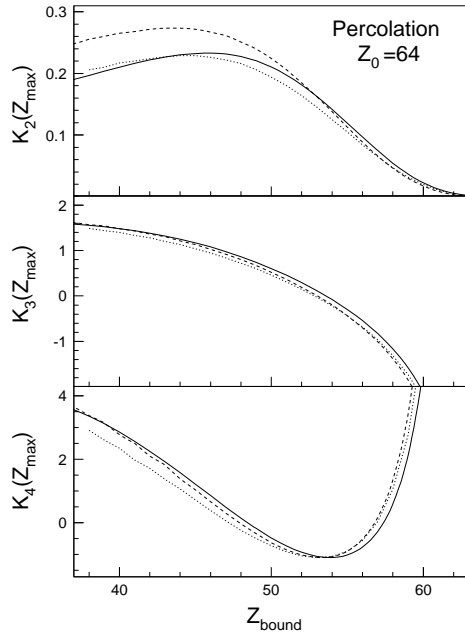


FIG. 5. The cumulants of $P(Z_{\max})$ as a function of Z_{bound} calculated for the system size $Z_0 = 64$ as shown in the left panel of Fig. 4 (full lines) in comparison with the results of the two tests described in the text investigating the effects of secondary decays (dashed lines) and of the detection efficiency of the spectrometer (dotted lines).

p_1 and p_2 indicate that K_2 significantly increases at small Z_{bound} while K_3 and K_4 remain nearly unchanged. As an example, for $Z_0 = 64$ with $p_1 = 0.6$ and $p_2 = 0.3$, the maximum of K_2 increases from 0.23 to 0.27 and its position is shifted towards lower Z_{bound} by $\sim 5\%$ (Fig. 5, dashed lines). These observations support the conclusion that K_3 and K_4 are more reliable than K_2 as quantitative indicators of the transition points.

The results of a test investigating the effects of the small detection inefficiencies of the spectrometer are shown in the same panels of Fig. 5 (dotted lines). It consisted of modifying the percolation event files by randomly deleting fragments with probabilities $1 - \epsilon(Z)$ and redoing the cumulant analysis with these modified files. The detection efficiencies $\epsilon(Z)$ were assumed to have the values of the geometrical acceptance of the time-of-flight wall of the spectrometer as determined for 800 MeV/nucleon incident energy [43]. They increase smoothly from $\epsilon(2) = 0.93$ to $\epsilon(7) = 0.99$ and $\epsilon(Z) = 1.00$ for $Z \geq 8$. This test cannot restore the original event structure nor can it take account of additional sources of uncertainties mentioned in the experimental reports [31, 43] as, e.g., reactions in the detector material.

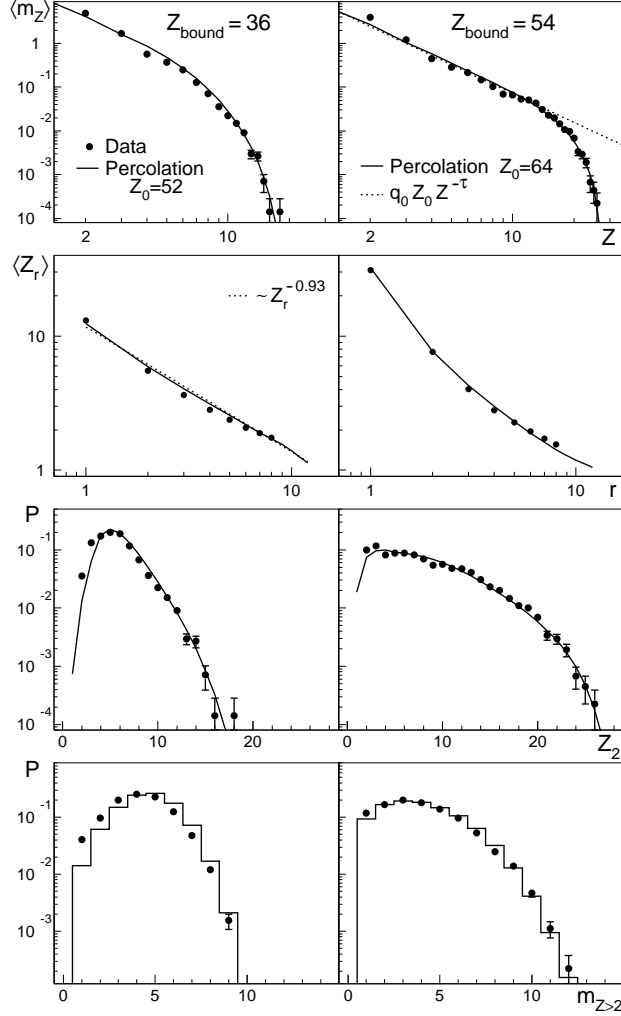


FIG. 6. Comparison of percolation predictions (full lines) for $Z_0 = 52$ (left panels) and $Z_0 = 64$ (right panels), with the experimental data for all systems (filled circles), selected with the conditions $Z_{\text{bound}} = 36$ and 54 , respectively. From top to bottom: the mean fragment multiplicity as a function of the fragment size Z (the largest fragment excluded), the mean fragment size as a function of the fragment rank r , the probability distribution of the size of the second largest fragment Z_2 , and the multiplicity distribution $m_{Z>2}$ of fragments with $Z > 2$. The dotted lines represent power-law descriptions as indicated. The statistical errors are shown where they are larger than the data symbols.

However, these processes are estimated to cause similarly small effects on the percent level whose magnitude can equally be estimated from the deviation of the test result. Both tests indicate that the modifications can be expected to be small, corresponding to an uncertainty of the order of one unit of Z_{bound} on the abscissa. The coincidence of the zero crossing of

K_3 with the minimum of K_4 is not affected.

The pairwise correspondence exhibited by the K_3 and K_4 cumulant ratios implies very similar $P(Z_{max})$ distributions but is even more general. A close resemblance between the whole fragmentation patterns is observed, as demonstrated in Fig. 6 for the data sets with $Z_{\text{bound}} = 36$ and 54. The percolation calculations are performed for the estimated system sizes $Z_0 = 52$ and 64, respectively. All the experimental data sets are summed for better statistics.

The top row of panels shows the fragment size distributions. The model describes the data rather well over four orders of magnitude. At $Z_{\text{bound}} = 54$, as expected for the percolation pseudocritical point, the distribution follows for $Z < 15$ the asymptotic power-law dependence with the exponent $\tau = 2.189$ and the normalization constant $q_0 = 0.173$ [25].

The next row shows the Zipf-type plots, i.e. the mean size of the largest, second largest, and up to the r^{th} -largest fragments plotted against their rank r . Such plots have been examined in the context of the expected appearance of Zipf's law near a critical point [6, 9, 44–47]. The Zipf's law states that $\langle Z_r \rangle \sim 1/r^\lambda$ with $\lambda \simeq 1$. The percolation results are shown for the rank numbers 1 to 11. The total fragment multiplicity m is at least 11 in all the percolation events. This is implied by the condition $m > Z_0 - Z_{\text{bound}}$. The experimental data contain information only on fragments with $Z > 1$. Since their mean multiplicities for $Z_{\text{bound}} = 36$ and 54 are about 9.1 and 7.7, the mean total multiplicities including $Z = 1$ isotopes may be estimated as 25.1 and 17.7, respectively, by assuming $m_{Z=1} = Z_0 - Z_{\text{bound}}$. It was, therefore, assumed that events containing less than 8 fragments can be supplemented with fragments of $Z = 1$ up to the rank of 8. At $Z_{\text{bound}} = 36$, one observes an approximate behavior according to Zipf's law with the exponent $\lambda \simeq 0.93$ determined from a fit to the percolation results. It is worthwhile to note that this feature appears at the “critical” point while a trace of the asymptotic power-law behavior in the fragment size distribution (with the largest fragment excluded) is observed at the pseudocritical point $Z_{\text{bound}} = 54$.

The percolation model very well describes not only mean values but also event-to-event fluctuations. As an example, the third row of panels of Fig. 6 shows the probability (yield fraction) distributions of the second largest fragment. The bottom row shows the multiplicity distributions of fragments with $Z > 2$. At $Z_{\text{bound}} = 36$ where the excitation energy is large, the calculated multiplicity distribution is shifted to values slightly larger than the experimental results while they practically coincide at $Z_{\text{bound}} = 54$.

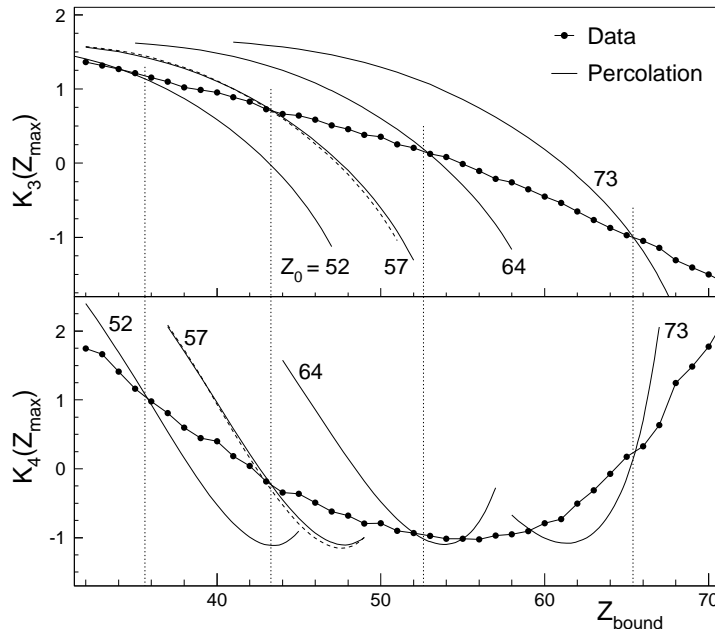


FIG. 7. The K_3 and K_4 cumulants as a function of Z_{bound} . The experimental data (filled circles, all systems, as shown by full lines in Fig. 4, right panel) and percolation calculations for the indicated system sizes Z_0 . The dotted vertical lines illustrate the identical crossing points for K_3 and K_4 , the dashed line shows the result obtained with a Gaussian distribution of Z_0 with $\langle Z_0 \rangle = 57$ (see text).

For such comparisons that can be extended to other Z_{bound} values, only the knowledge of the relation between Z_{bound} and Z_0 is required. Here, this relation is determined on the basis of the K_3 and K_4 equalities. The analysis can also be performed in a slightly different manner. In Fig. 7 the cumulants are plotted as a function of Z_{bound} for the experimental data and percolation systems of different sizes. For a given Z_0 , the crossing of the percolation and experimental lines determine the corresponding Z_{bound} . The relation found by this procedure is displayed in Fig. 3 by the solid circles. It shows good agreement with the experimental estimates of Ref. [41].

In reality, the system sizes at fixed Z_{bound} are dispersed. To evaluate the significance of this dispersion for the analysis, percolation calculations have been performed for a Gaussian distribution of Z_0 with the mean of 57 and standard deviation of 2. Such a deviation is suggested by SMM simulations performed with input conditions established in Ref. [48]. The results are plotted in Fig. 7 by the dashed lines, showing that the dispersion effects are not substantial.

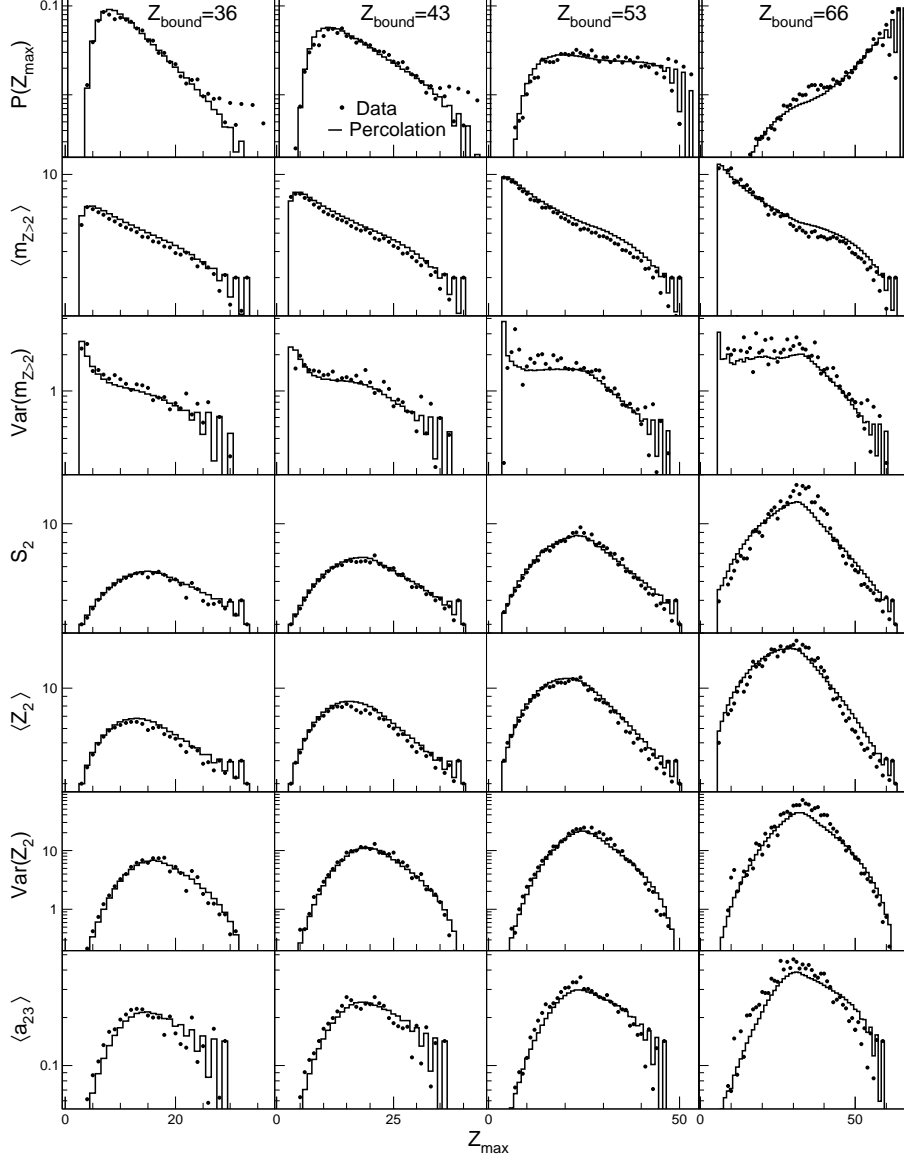


FIG. 8. Percolation (solid histograms) vs experimental data (dots, all systems): characteristics of fragments with $Z > 2$ are plotted as a function of Z_{max} . From top to bottom: the Z_{max} distribution, the mean and variance of the fragment multiplicity, the mean fragment size, the mean and variance of the second largest fragment size, the mean size asymmetry between the second and third largest fragments. The statistical errors are of the order of the scatter of the data symbols.

The model predictions are examined in more detail in Fig. 8. The comparisons are made at the matching conditions determined from Fig. 7. To not obscure the histograms, error bars are omitted in the figure. Their magnitude is evident from the scatter of the data symbols. The top diagrams show the $P(Z_{max})$ distributions. Overall, the agreement is very

good, although the experimental distributions exhibit some local enhancements which are not accounted for by the model. They are seen for $Z_{\text{bound}} = 36$ and 43 at largest Z_{max} , which corresponds to events with one large fragment and few light particles. Such evaporation-like events are not unexpected even for large excitation energies, since neutron-rich projectile spectators can be cooled by neutron emissions. Another enhancement which is seen at $Z_{\text{bound}} = 66$ near $Z_{\text{max}} \simeq 36$ is most likely associated with a contribution from fission events.

The next panels in Fig. 8 examine various fragment size characteristics and correlations as a function of Z_{max} . They are the mean and variance of the multiplicity of fragments with $Z > 2$, the mean fragment size S_2 defined as the second moment of the fragment size distribution normalized to the first moment (the largest fragment excluded) [35], the mean and variance of the second largest fragment size, and the size asymmetry between the second and third largest fragments $a_{23} \equiv (Z_2 - Z_3)/(Z_2 + Z_3)$ averaged over events with $Z_3 > 2$. In these calculations only fragments with $Z > 2$ are taken into account to avoid contributions from light particles coming from other sources.

One may ask whether simultaneously fixed Z_{bound} and Z_{max} will severely limit the possibilities for the fragment-size partitioning, leading to rather trivial results. This is the case when Z_{max} is close to its limiting minimum or maximum value. The number of possible partitions is largest for Z_{max} in the middle of its range, around $Z_{\text{bound}}/2$. This least restrictive condition allows for a better test of fragmentation patterns. Without additional Z_{max} selection the characteristics would be dominated by the trivial contributions in the cases when $P(Z_{\text{max}})$ distributions are peaked near the limiting Z_{max} values (cf. top rows of Fig. 8).

This very detailed quantitative analysis confirms that the bond percolation model remarkably well describes the experimental fragment sizes and their fluctuations. This has been noticed early on after the first ALADIN data on projectile fragmentation had become available and was reported for a set of fragment distributions and asymmetries in Ref. [32]. The percolation results may serve as a reference for further analysis with other models and for sensitive tests of their performance. In fact, calculations performed with the lattice-gas model and with the SMM have shown that the characteristic coincidence of the zero transition of the skewness and the minimum of the kurtosis excess is observed with these models as well [24, 49]. Considered as indicators for a second-order phase transition, they are simultaneously present in these statistical models that are believed to exhibit a phase transition of first-order in the thermodynamic limit.

The cumulant analysis indicates $Z_{\text{bound}} = 54$ as the transition point for nuclear systems with $Z_0 \simeq 64$. Based on estimations performed for the $^{197}\text{Au} + ^{197}\text{Au}$ reaction at 600 MeV/nucleon [31, 41], this point corresponds to the excitation energy around 6 MeV per nucleon, which can be associated with a temperature within the range 5–7 MeV [41, 50, 51]. In the percolation context, the transition point can be interpreted as the pseudocritical point. The analysis suggests that near-critical events are rather located at $Z_{\text{bound}} \simeq 36$ for which the estimated excitation energy is about 10 MeV per nucleon, corresponding to temperatures in the range 6 to 7 MeV. These temperatures are much lower than the critical temperature of about 14 – 15 MeV, calculated with relativistic mean-field models for asymmetric nuclear matter with a proton fraction of the ^{197}Au nucleus [52, 53]. However, in finite nuclear systems the critical temperature can be reduced by more than 5 MeV due to the presence of the Coulomb and surface effects [54]. The estimated temperatures depend on the method and the size of the studied system. For example, according to calculations with the Fermionic Molecular Dynamics model performed for ^{16}O , the critical temperature deduced from observing the disappearance of the liquid-gas coexistence is about 10 MeV [55]. A somewhat larger value $T_c \simeq 12$ MeV has been concluded from a study of a system of mass number $A = 36$ with antisymmetrized molecular dynamics [56].

V. DISCUSSION

A. Shapes of the Z_{max} distributions and Δ -scaling

The behavior of the cumulants is of interest in the context of Δ -scaling proposed for studying criticality in finite systems [1, 57, 58]. Probability distributions $P(s_{\text{max}})$ of the extensive order parameter s_{max} for different “system sizes” $\langle s_{\text{max}} \rangle$ obey Δ -scaling if they can be converted to a single scaling function $\Phi(z_{(\Delta)})$ by the transformation

$$\langle s_{\text{max}} \rangle^\Delta P(s_{\text{max}}) = \Phi(z_{(\Delta)}) \equiv \Phi\left(\frac{s_{\text{max}} - \langle s_{\text{max}} \rangle}{\langle s_{\text{max}} \rangle^\Delta}\right), \quad (2)$$

where $1/2 \leq \Delta \leq 1$.

The Δ -scaling method has been applied to distributions of the largest fragment charge with expectations that the distributions obey the $\Delta = 1/2$ scaling in the ordered (low temperature) phase and the $\Delta = 1$ scaling in the disordered (high temperature) phase

[1, 5, 6, 8, 19]. The transition between the two scaling regimes would signal the presence of a phase transition. The percolation model contradicts such expectations [25]. In the percolation disordered phase no Δ -scaling is observed for the largest cluster size. Concerning the ordered phase, the $\Delta = 1/2$ scaling can only be observed for different system sizes at a fixed value of the control parameter. This requirement is difficult to realize experimentally. Moreover, in systems of small sizes corresponding to nuclear systems, this limiting scaling behavior is violated as a consequence of surface effects.

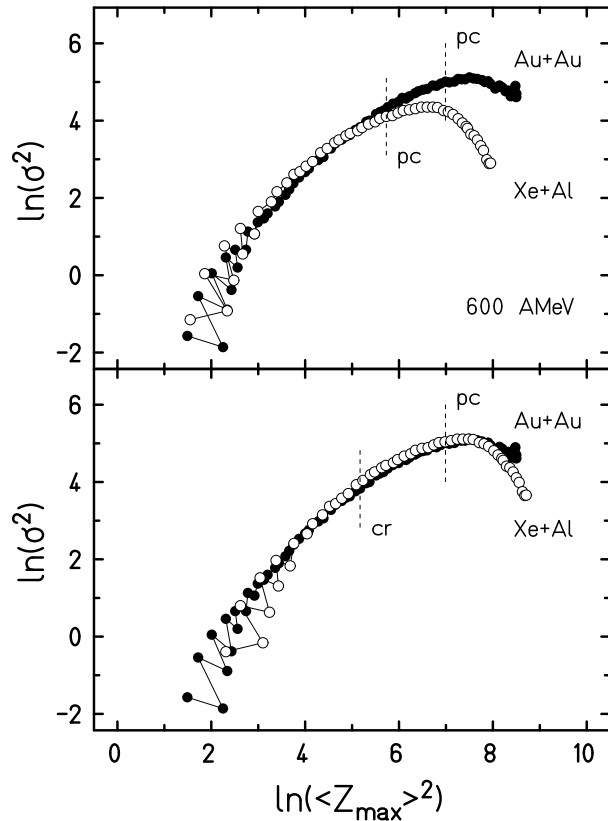


FIG. 9. Natural logarithm of the variance as a function of the natural logarithm of the squared mean value of the largest atomic number Z_{\max} recorded in $^{197}\text{Au} + ^{197}\text{Au}$ (filled circles) and $^{131}\text{Xe} + ^{27}\text{Al}$ collisions (open circles) at 600 MeV/nucleon (top panel) and after shifting of the ^{131}Xe data with the value 0.76 in both dimensions (see text). The data symbols represent the results for individual values of Z_{bound} in the range from 4 to $Z_{\text{proj}} + 1$. The positions of the pseudocritical points are indicated for the two systems in the top panel, and the critical (cr) and pseudocritical (pc) points for $^{197}\text{Au} + ^{197}\text{Au}$ are given in the bottom panel (dashed vertical lines).

The present experimental data with events sorted according to Z_{bound} do not show Δ -

scaling features in any Z_{bound} range. This can be concluded from Fig. 4, considering that $K_3 = \text{const}$ and $K_4 = \text{const}$ are necessary conditions for Δ -scaling [25]. Another condition required for Δ -scaling is a linear correlation of the natural logarithms of the variance and squared mean value of the variable considered as an order parameter. This correlation is shown in Fig. 9 for the experimental results for $^{197}\text{Au} + ^{197}\text{Au}$ and $^{131}\text{Xe} + ^{27}\text{Al}$ collisions, both at 600 MeV/nucleon and after sorting according to Z_{bound} . The positions of the pseudocritical points are indicated in the top panel of the figure. For $^{197}\text{Au} + ^{197}\text{Au}$, the corresponding Z_{bound} is directly taken from Fig. 4. For $^{131}\text{Xe} + ^{27}\text{Al}$, the pseudocritical Z_{bound} reported for $^{124}\text{Sn} + \text{Sn}$ in Ref. [49] was used and a 8% correction was applied corresponding to the ratio of the atomic numbers of the Xe and Sn projectiles.

The similarity of the two correlations is even better appreciated if the $^{131}\text{Xe} + ^{27}\text{Al}$ result is scaled according to the atomic numbers Z of the Au and Xe projectiles. Their ratio 79/54 that enters squared in the arguments of the logarithms leads to a linear shift by 0.76 in both, x and y , dimensions (Fig. 9, bottom panel). The similarity of the two functions reflects the invariance with respect to the projectile Z that was observed for the fragment multiplicities and correlations in Ref. [31]. The smooth variation of the slopes of the correlations is very similar to the percolation result reported in Fig. 7 of Ref. [25]. On the basis of the observed near perfect descriptions of the experimental data with percolation (cf. Figs. 6 and 8), even the remarkable quantitative agreement is not surprising. The location of the turnover at $\ln(\langle Z_{\text{max}} \rangle^2) \simeq 7$ and $\ln(\sigma^2) \simeq 5$ near the pseudocritical point is well reproduced. The observed experimental correlation is also similar to the results reported in Ref. [5] for the Xe+Sn reactions at incident energies between 25 and 50 MeV/nucleon (Fig. 4 of Ref. [5]). With these reactions, after sorting according to the measured total transverse energy of light charged particles, an interval of approximately $5.4 < \ln(\langle Z_{\text{max}} \rangle^2) < 7.6$ was covered while, in the present case, the correlation extends as far down as $\ln(\langle Z_{\text{max}} \rangle^2) \simeq 2$. The definition of Z_{bound} causes the staggering that is observed there for the very small values of Z_{bound} .

The trend towards positively skewed Z_{max} distributions expected in the disordered regime is approximately realized, both in the experimental data and in the percolation model describing them. The asymptotic value $K_3 \simeq 1.6$ of the skewness for small Z_{bound} (Fig. 4) or large bond-breaking probabilities p_b (Fig. 1) is larger than the $K_3 = 1.14$ of the Gumbel distribution in the continuous limit but of the same order of magnitude. The Gumbel distribution permits rather satisfactory descriptions of the experimental Z_{max} probability

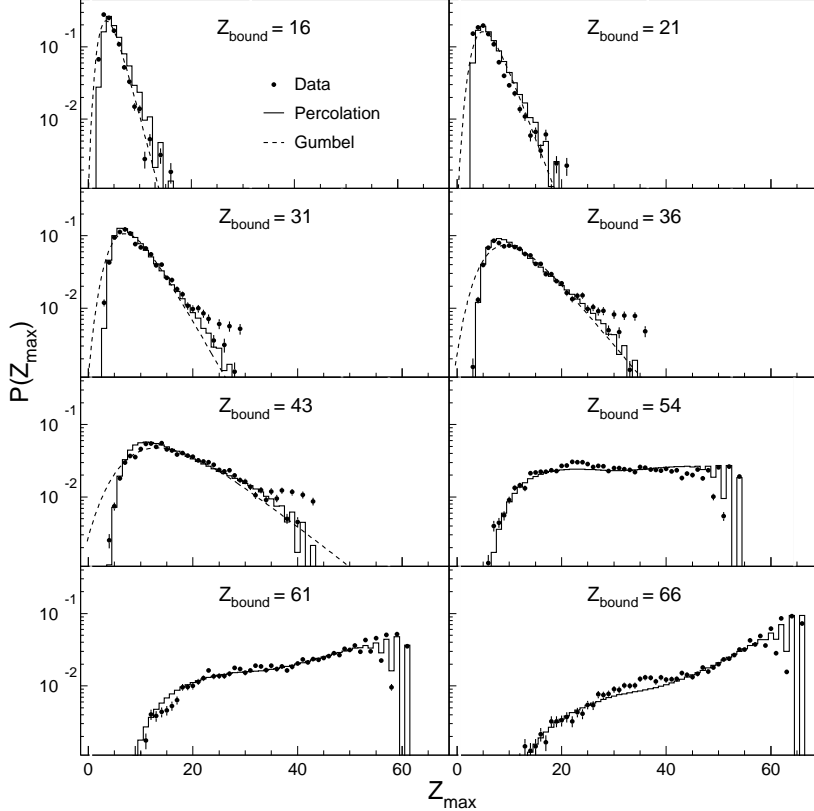


FIG. 10. Probability distributions $P(Z_{\max})$: comparison of percolation results (histograms) for the indicated values of Z_{bound} with the experimental data for all systems (filled circles) and with Gumbel distributions fitted to the experimental data for the cases $Z_{\text{bound}} \leq 43$ (dashed lines).

distributions in this range of Z_{bound} as illustrated in Fig. 10 for selected cases. Only the sharp drop of the distribution at small Z_{\max} cannot be reproduced. The calculations were performed for system sizes $Z_0 = 31, 36, 48, 52, 57, 64, 70$, and 73 for $Z_{\text{bound}} = 16, 21, 31, 36, 43, 54, 61$, and 66 , respectively.

In Ref. [5], scaling has been further studied for the recorded most central collisions as a function of the bombarding energy. For $^{197}\text{Au} + ^{197}\text{Au}$ at incident energies 40 to 80 MeV/nucleon, a linear scaling with $\Delta = 1$ has been observed (Fig. 13 in Ref. [5]). This trend is qualitatively continued by the present data taken at 600 MeV/nucleon. If extended to $\ln(\langle Z_{\max} \rangle^2) \simeq 2$, the linear fit shown in that figure will reach $\ln(\sigma^2) \simeq -1$, there coinciding with the most central bins of the present data set (Fig. 9). Gaussian distributions are, however, not observed here. At small p_b , neither the skewness nor the kurtosis excess do approach the vanishing values $K_3 = K_4 = 0$ characterizing the Gaussian distribution

(Figs. 1 and 4). The Gaussian distribution is reached as the asymptotic value with bond percolation only in the continuous limit or for large systems with periodic boundary conditions [25]. The experimental situation is dominated by the transition to negatively skewed Z_{\max} distributions (Fig. 10). At very large Z_{bound} , corresponding to smaller excitation energies in the experiment, the partitioning probability decreases approximately exponentially with decreasing Z_{\max} . This is well reproduced with percolation.

B. Remarks on bimodality

Bimodality in distributions of the largest fragment size or other quantities expected to be closely correlated with the order parameter is considered as a promising signature of first-order phase transition [18, 59, 60]. Experimental examinations of the largest-fragment charge distribution have, however, not ascertained yet such a signal up to now. The presence of bimodality has been reported for distributions of some other quantities as, e.g., the charge asymmetry between the two or three largest fragments, and the asymmetry ratio between heavy and light fragments [6, 8, 17, 18, 61]. In the ALADIN data on $^{197}\text{Au} + ^{197}\text{Au}$ at 1000A MeV, a bimodal distribution of $Z_{\max} - Z_2 - Z_3$ has been found in the transition region $Z_{\text{bound}} = 53 - 55$ [18, 62]. The bimodal behavior of this variable is also observed in bond percolation in which only a second-order phase transition is present. It has been identified as a finite-size effect obeying a power-law with the known value $\nu = 0.88$ [35] of the critical exponent describing the divergence of the correlation length [62].

As expected for the continuous percolation transition, the distribution of Z_{\max} does not exhibit bimodality. The shape of the transitional distribution is characterized by a wide plateau as illustrated in Fig. 2(a) and Fig. 11. Such characteristics are observed when events are sorted according to the control parameter p_b . If p_b is dispersed in a sample of events, the shape of $P(Z_{\max})$ can be very different. In particular, a bimodal shape may be observed as illustrated in Fig. 11. It serves as a warning against using wide bins for event sorting (see, e.g., Ref. [63]) or sorting variables that are not well correlated with the control parameter.

The latter applies to the study of projectile fragmentation in $^{197}\text{Au} + ^{197}\text{Au}$ collisions at energies between 60 and 100 MeV/nucleon that reported on bimodal behavior of the heaviest-fragment distributions [10]. Since a strict canonical sampling is not possible in the

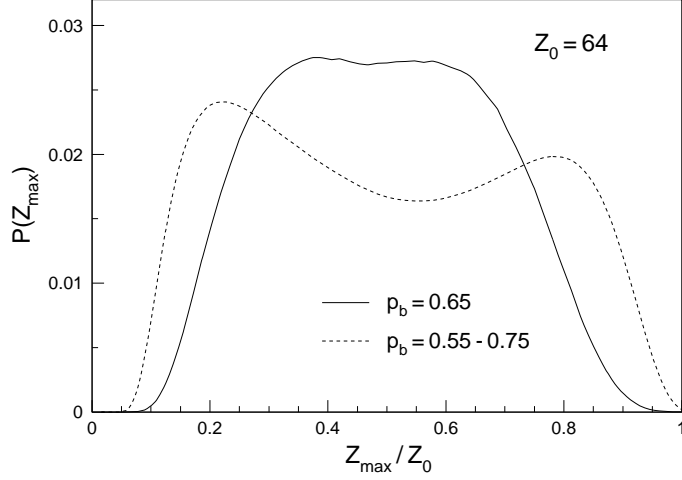


FIG. 11. Bond percolation for $Z_0 = 64$. The probability distribution of Z_{max} at the transition point $p_b = 0.65$ (solid line) and for the bond probability distributed over a finite range (dashed line).

experiment a scheme of selecting and weighting event groups has been applied with the aim to generate equivalent-to-canonical data samples. The obtained enhancements of the Z_{max} distributions at values of $0.9 Z_0$ and $0.3 Z_0$ with excitation energies below 2 and above 8 MeV/nucleon, respectively, correspond to residue production in peripheral collisions and in highly fragmented processes at the threshold to vaporization. Without the strict sorting conditions that have been applied, these event groups will be characterized by rather different temperatures and system sizes. The reported observations, based on retaining only tails of their distributions, thus represent the studied reactions only very indirectly [64].

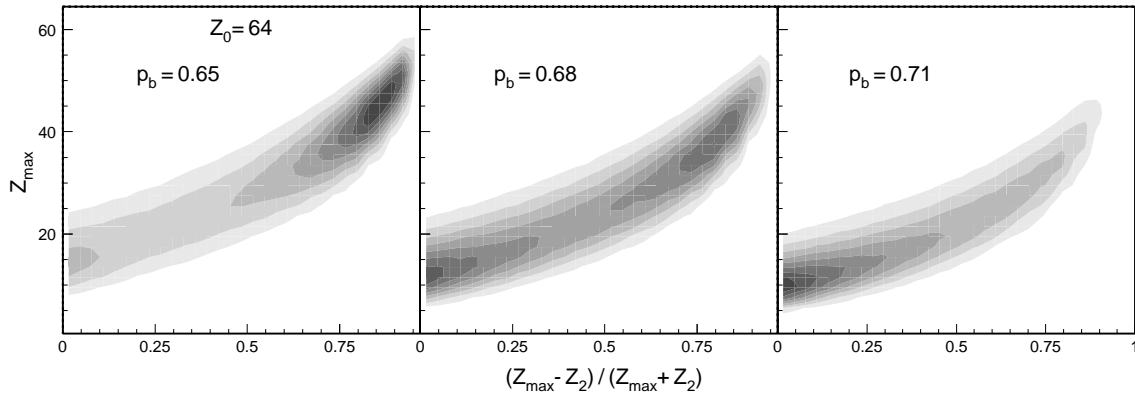


FIG. 12. Bond percolation for $Z_0 = 64$. Correlations between Z_{max} and the size asymmetry of the two largest clusters in the transition region.

Even when percolation events are sorted by the control parameter, various size asymmetry variables exhibit bimodal behavior in the transition region. As an example, Fig. 12 shows the correlation between Z_{max} and the size asymmetry of the two largest fragments $(Z_{max} - Z_2)/(Z_{max} + Z_2)$. A bimodal structure of this distribution is clearly observed at $p_b = 0.68$. It should be noted that the projection onto the Z_{max} axis does not reveal this bimodality. A similar degree of bimodality is observed for a much larger system with 16^3 sites, suggesting that this feature is not generated by finite size effects. Correlations of this kind were examined experimentally for fragmentation of projectiles in $^{197}\text{Au} + ^{197}\text{Au}$ and $\text{Xe} + \text{Sn}$ reactions at 80 MeV/nucleon with qualitatively similar results [8].

Another example concerns the asymmetry between the total sizes of large and small fragments. Following the prescription applied to $\text{Xe} + \text{Sn}$ central collisions [17], fragments with $Z \geq 13$ are considered as large and fragments with $3 \leq Z \leq 12$ as small. The evolution of their normalized difference distributions near the percolation transition is illustrated in the left diagram of Fig. 13. The system size of 100 sites is comparable to the total charge of the investigated nuclear system. Also in this case a bimodal structure is predicted by the percolation model. The right diagram shows the qualitatively similar result that is observed when the clusters with $Z = 1 - 2$ are additionally included in the group of light fragments.

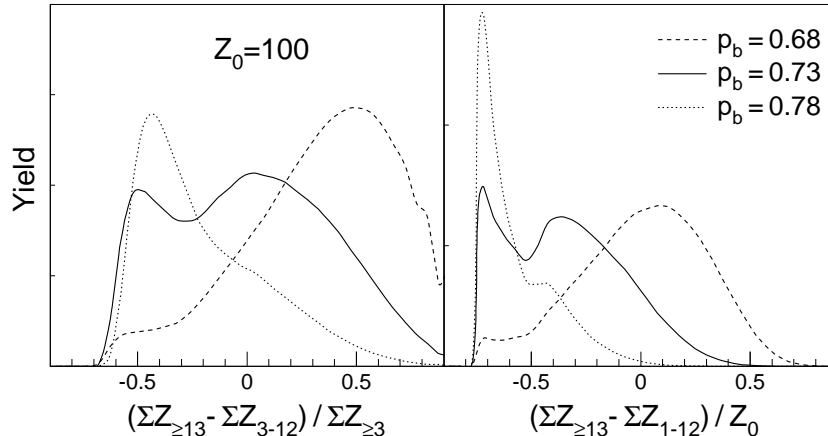


FIG. 13. Bond percolation for $Z_0 = 100$: distributions of the normalized differences between the sum of atomic numbers of large fragments with $Z \geq 13$ and the sum of atomic numbers of small fragments with $3 \leq Z \leq 12$ (left panel) or with $1 \leq Z \leq 12$ (right panel), calculated for three values of the bond breaking probability p_b below, near, and above the pseudocritical point.

The presented percolation simulations demonstrate that bimodalities observed in distri-

butions of the asymmetry variables are not necessarily associated with a first-order phase transition. A similar conclusion was reached in Ref. [65] based on calculations with the quantum-molecular dynamics transport model for $^{197}\text{Au} + ^{197}\text{Au}$ collisions. There the authors concluded that fluctuations introduced by elementary nucleon-nucleon collisions cause the bifurcation observed in the distributions of fragment-charge asymmetries. Given the good reproduction even of the higher-order distribution parameters, these effects are realistically also included in the percolation description.

C. Critical behavior in the coexistence zone

The simultaneous appearance of signals expected for first- and second-order phase transitions in finite systems is known since long ago [7, 22, 23, 39]. It has very recently been discussed again by investigating the lattice-gas model in addition to the percolation and thermodynamic models used here (cf. Figs. 1 and 2) [66]. All three models were shown to provide qualitative descriptions of experimental data while the transition points are indicative of either a first- or a second-order transition, depending on the model that is applied.

A possible solution to the puzzle appeared when calculations with the lattice-gas model demonstrated the existence of critical-like regions within the coexistence zone of the phase diagram [3, 7, 22–24]. Scaling behavior was observed along a line that, in the case of small systems, extends from near the thermodynamical critical point of the phase diagram toward lower temperatures and lower densities into the coexistence region. It appears as an extension of the so-called Kertész line that is observed in lattice-gas and molecular-dynamics models at temperatures and densities above their critical points [20, 21, 67].

According to the lattice-gas applications to fragmentation reactions, the associated critical temperatures are of the order of 5 MeV [24] or 6 to 8 MeV [23], i.e. far below the expected critical temperature in a temperature-vs-density phase diagram, even for small systems (cf., e.g., Refs [54–56]). As noticed by Le Neindre *et al.*, these temperatures are comparable to the critical temperatures appearing in analyses based on Fisher scaling [9]. In fact, the values reported in Refs. [68–70] are between 4.75 and about 8 MeV. Apparently, the "critical" disassemblies identified by searching for the scaling features of power-law type fragment spectra are located at or near the extension of the Kertész line into the coexistence zone. The observed broad range of reported temperatures is to be expected because

different reaction types and experimental techniques will lead to different approaches of the critical line or region. There are, in addition, the uncertainties associated with determining temperatures from the observed fragment properties and yields.

Also in the case studied here, the location of the line of critical-like behavior in a temperature vs density phase diagram is rather uncertain. However, the precision observed for the reproduction of fluctuation properties of percolation up to fourth order is remarkable. Campi *et al.*, in their search for generic properties of the fragmentation of simple fluids, argue that the random breaking of bonds may be the simplest explanation for the appearance of percolation features in nuclear fragmentation [15]. The nucleon-nucleon collision dynamics introduces the required stochastic element in the present case of spectator fragmentation at relativistic energies. In their later study [67], based on classical molecular dynamics calculations, the same authors have presented a scenario that involves the out-of-equilibrium expansion of the system, starting from an equilibrium configuration outside the coexistence zone. As the calculations show, the compositions generated at an early, high density stage are largely preserved in the final state. Systems expanding from near the percolation critical region, the Kertész line in infinite systems, may thus appear with critical properties. In an alternative scenario, the excited spectator matter equilibrates faster than it expands and cools, reaching the coexistence zone [55]. Quantum-molecular-dynamics calculations that reproduce the experimental fragmentation patterns, may be capable of shedding more light on these possibilities.

VI. CONCLUSIONS

The analysis of the ALADIN data on fragmentation processes of ^{197}Au projectiles on heavy targets at energies between 600 and 1000 MeV/nucleon has been focused on the fluctuations of the largest fragment size (charge or atomic number Z). Cumulants of the largest fragment size distribution were examined as a function of Z_{bound} . Particularly valuable measures are the higher-order cumulants, skewness K_3 and kurtosis excess K_4 . The transitional distribution indicated by $K_3 = 0$ and a minimum of K_4 is characteristic of a phase transition. In percolation, it corresponds to the pseudocritical point, and in a thermodynamic model, to the maximum of the specific heat that is associated with a first-order transition. Such a transition point is observed at $Z_{\text{bound}} \simeq 54$ which, according to Ref. [41], corresponds

to excitation energies near 6 MeV/nucleon, associated with a temperature between 5 and 7 MeV.

The cumulants K_3 and K_4 may be used as constraints for comparisons with model predictions when system sizes are not unequivocally determined. They are shown to be not significantly affected by experimental conditions and secondary decay effects. Such constraints have been applied in the comparisons made with the bond percolation model, intended to test the whole fragmentation pattern.

Fragment sizes and their event-to-event fluctuations observed in the experiment are remarkably well reproduced by the bond percolation model. The system sizes determined from the percolation analysis are found to be in good agreement with experimental estimates. The analysis suggests that near-critical events, corresponding to the true critical point, are located at $Z_{\text{bound}} \simeq 36$. The associated excitation energy is about 10 MeV/nucleon, leading to a percolation critical temperature of again, approximately 6 to 7 MeV [41, 51].

Owing to the high accuracy in describing the fragment-size properties, the simple percolation model, containing a second-order phase transition, may still serve as a very useful reference model for studying the phase behavior of fragmenting systems. In particular, it permits verifying the uniqueness of signatures proposed for revealing the presence of a first-order phase transition. It needs to be stressed, however, that model comparisons, to be applicable for an experimental verification, should rely on event samples selected with measurable quantities. These sorting quantities are inevitably dispersed over the control parameter of the model as, e.g., the temperature or the bond probability, which may significantly modify the expected signatures.

ACKNOWLEDGMENTS

The authors would like to express their gratitude to the ALADIN Collaboration for the permission to use the event-sorted fragmentation data of experiment S114. This work was supported by the Polish Scientific Research Committee, Grant No. 2P03B11023.

[1] R. Botet, M. Płoszajczak, A. Chbihi, B. Borderie, D. Durand, and J. Frankland, *Phys. Rev. Lett.* **86**, 3514 (2001).

- [2] R. Botet and M. Płoszajczak, *Universal Fluctuations: The Phenomenology of Hadronic Matter*, in: World Scientific Lecture Notes in Physics, Vol. 65, World Scientific Publishing, Singapore, 2002.
- [3] J. M. Carmona, J. Richert, and P. Wagner, *Phys. Lett. B* **531**, 71 (2002).
- [4] Yingxun Zhang, Xizhen Wu, and Zhuxia Li, *Phys. Rev. C* **69**, 044609 (2004).
- [5] J. D. Frankland *et al.*, *Phys. Rev. C* **71**, 034607 (2005).
- [6] Y. G. Ma *et al.*, *Phys. Rev. C* **71**, 054606 (2005).
- [7] F. Gulminelli and Ph. Chomaz, *Phys. Rev. C* **71**, 054607 (2005).
- [8] M. Pichon *et al.*, *Nucl. Phys.* **A779**, 267 (2006).
- [9] N. Le Neindre *et al.*, *Nucl. Phys.* **A795**, 47 (2007).
- [10] E. Bonnet *et al.*, *Phys. Rev. Lett.* **103**, 072701 (2009).
- [11] X. Campi, *Phys. Lett. B* **208**, 351 (1988).
- [12] J. Brzychczyk *et al.*, *Phys. Rev. C* **58**, R1372 (1998).
- [13] C. O. Dorso, V. C. Latora, and A. Bonasera, *Phys. Rev. C* **60**, 034606 (1999).
- [14] J. B. Elliott *et al.*, *Phys. Rev. C* **62**, 064603 (2000).
- [15] X. Campi, H. Krivine, N. Sator, and E. Plagnol, *Eur. Phys. J. D* **11**, 233 (2000).
- [16] G. Chaudhuri and S. Das Gupta, *Phys. Rev. C* **76**, 014619 (2007).
- [17] B. Borderie, *J. Phys. G: Nucl. Part. Phys.* **28**, R217 (2002).
- [18] O. Lopez and M. F. Rivet, *Eur. Phys. J. A* **30**, 263 (2006)
- [19] D. Gruyer *et al.*, *Phys. Rev. Lett.* **110**, 172701 (2013).
- [20] J. Kertész, *Physica* **A161**, 58 (1989).
- [21] X. Campi and H. Krivine, *Nucl. Phys.* **A620**, 46 (1997).
- [22] F. Gulminelli and Ph. Chomaz, *Phys. Rev. Lett.* **82**, 1402 (1999).
- [23] C. B. Das *et al.*, *Phys. Rev. C* **66**, 044602 (2002).
- [24] A. Wieloch, J. Brzychczyk, J. Łukasik, P. Pawłowski, T. Pietrzak, and W. Trautmann, in *Proceedings of the IWM2009 International Workshop on Multifragmentation and Related Topics*, Catania, Italy, edited by J. D. Frankland, A. Pagano, S. Pirrone, M-F. Rivet, and F. Rizzo (Conference Proceedings Vol. 101, Italian Physical Society, Bologna 2010), p. 158; preprint arXiv:nucl-th/1003.2794.
- [25] J. Brzychczyk, *Phys. Rev. C* **73**, 024601 (2006).
- [26] M. A. Stephanov, *Phys. Rev. Lett.* **107**, 052301 (2011).

- [27] K. Redlich, *Cent. Eur. J. Phys.* **10**, 1254 (2012).
- [28] M. Asakawa and M. Kitazawa, *Progr. Part. Nucl. Phys.* **90**, 299 (2016).
- [29] Z. Fecková, J. Steinheimer, B. Tomášik, and M. Bleicher, *Phys. Rev. C* **93**, 054906 (2016).
- [30] V. Vovchenko, D. V. Anchishkin, M. I. Gorenstein, and R. V. Poberezhnyuk, *Phys. Rev. C* **92**, 054901 (2015).
- [31] A. Schüttauf *et al.*, *Nucl. Phys.* **A607**, 457 (1996).
- [32] P. Kreuzt *et al.*, *Nucl. Phys.* **A556**, 672 (1993).
- [33] S. Das Gupta and A. Z. Mekjian, *Phys. Rev. C* **57**, 1361 (1998).
- [34] C. B. Das, S. Das Gupta, W. G. Lynch, A. Z. Mekjian, and M. B. Tsang, *Phys. Rep.* **406**, 1 (2005).
- [35] D. Stauffer and A. Aharony, *Introduction to percolation theory*, 2nd Edition, (Taylor & Francis, London, 1992).
- [36] W. Bauer, D. R. Dean, U. Mosel, and U. Post, *Phys. Lett. B* **150**, 53 (1985).
- [37] J. Hoshen and R. Kopelman, *Phys. Rev. B* **14**, 3438 (1976).
- [38] J. P. Bondorf, A. S. Botvina, A. S. Iljinov, I. N. Mishustin, and K. Sneppen, *Phys. Rep.* **257**, 133 (1995).
- [39] K. A. Bugaev, M. I. Gorenstein, I. N. Mishustin, and W. Greiner, *Phys. Lett. B* **498**, 144 (2001).
- [40] J. Hubele *et al.*, *Z. Phys. A* **340**, 263 (1991).
- [41] J. Pochodzalla *et al.*, *Phys. Rev. Lett.* **75**, 1040 (1995).
- [42] X. Campi, H. Krivine, and E. Plagnol, *Phys. Rev. C* **50**, R2680 (1994).
- [43] A. Schüttauf, Ph.D. thesis, Universität Frankfurt am Main, 1996.
- [44] Y. G. Ma, *Phys. Rev. Lett.* **83**, 3617 (1999); *Eur. Phys. J. A* **6**, 367 (1999).
- [45] A. Dabrowska *et al.*, *Acta Phys. Pol. B* **35**, 2109 (2004).
- [46] X. Campi and H. Krivine, *Phys. Rev. C* **72**, 057602 (2005).
- [47] K. Paech, W. Bauer, and S. Pratt, *Phys. Rev. C* **76**, 054603 (2007).
- [48] A. S. Botvina *et al.*, *Nucl. Phys.* **A584**, 737 (1995).
- [49] T. Pietrzak *et al.*, in *Proceedings of the IWM2009 International Workshop on Multifragmentation and Related Topics*, Catania, Italy, edited by J. D. Frankland, A. Pagano, S. Pirrone, M-F. Rivet, and F. Rizzo (Conference Proceedings Vol. 101, Italian Physical Society, Bologna 2010), p. 171; preprint arXiv:nucl-ex/1003.2800.

- [50] J. B. Natowitz, R. Wada, K. Hagel, T. Keutgen, M. Murray, A. Makeev, L. Qin, P. Smith, and C. Hamilton, *Phys. Rev. C* **65**, 034618 (2002).
- [51] W. Trautmann *et al.*, *Phys. Rev. C* **76**, 064606 (2007).
- [52] Horst Müller and Brian D. Serot, *Phys. Rev. C* **52**, 2072 (1995).
- [53] Guang-Hua Zhang, Wei-Zhou Jiang, *Phys. Lett. B* **720**, 148 (2013).
- [54] H. R. Jaqaman, A. Z. Mekjian, and L. Zamick, *Phys. Rev. C* **29**, 2067 (1984).
- [55] J. Schnack and H. Feldmeier, *Phys. Lett. B* **409**, 6 (1997).
- [56] T. Furuta and A. Ono, *Phys. Rev. C* **74**, 014612 (2006).
- [57] R. Botet and M. Płoszajczak, *Phys. Rev. E* **62**, 1825 (2000).
- [58] R. Botet and M. Płoszajczak, *Nucl. Phys. B (Proc. Suppl.)* **92**, 101 (2001).
- [59] Ph. Chomaz, F. Gulminelli, V. Duflot, *Phys. Rev. E* **64**, 046114 (2001).
- [60] D.H.E. Gross, *Eur. Phys. J. A* **30**, 293 (2006), and in *Dynamics and Thermodynamics with Nuclear Degrees of Freedom*, ed. by Ph. Chomaz et al., Springer, Berlin Heidelberg New York, 2006.
- [61] N. Bellaize *et al.*, *Nucl. Phys.* **A709**, 367 (2002).
- [62] W. Trautmann *et al.* in *Proceedings of the XLVth International Winter Meeting on Nuclear Physics, Bormio, Italy*, edited by I. Iori and A. Tarantola (Ricerca Scientifica ed Educazione Permanente Suppl. No. 127, Milano, 2007), p. 205.
- [63] A. Le Fèvre *et al.*, *Phys. Rev. C* **80**, 044615 (2009).
- [64] S. Mallik, G. Chaudhuri, and F. Gulminelli, *Phys. Rev. C* **97**, 97, 024606 (2018).
- [65] A. Le Fèvre and J. Aichelin, *Phys. Rev. Lett.* **100**, 042701 (2008).
- [66] S. Das Gupta, S. Mallik, G. Chaudhuri, *Phys. Rev. C* **97**, 044605 (2018).
- [67] X. Campi, H. Krivine, E. Plagnol, and N. Sator, *Phys. Rev. C* **67**, 044610 (2003).
- [68] M. Kleine Berkenbusch *et al.*, *Phys. Rev. Lett.* **88**, 022701 (2002).
- [69] J. B. Elliott *et al.*, *Phys. Rev. Lett.* **88**, 042701 (2002).
- [70] J. B. Elliott *et al.*, *Phys. Rev. C* **67**, 024609 (2003).